PCCP

Accepted Manuscript

ROYAL SOCIETY OF CHEMISTRY

www.rsc.org/pccp

Phys. Chem. Chem. Phys

ARTICLE

Fe_3O_4 and Au nanoparticles dispersed on graphene support as a highly active catalyst toward the reduction of 4-nitrophenol

Received 00th January 20xx,
Accepted 00th January 20xx

DOI: 10.1039/x0xx00000x

www.rsc.org/

Yan Wang,* Hai Li, Jijun Zhang, Xinyu Yan and Zexiang Chen*

We report a highly efficient and reusable bifunctional nanostructured composite catalyst synthesized by a scalable facile hydrothermal method which enables precise control of size and morphology of nanoparticles, wherein Au nanoparticles (NPs) and Fe_3O_4 particles exhibits excellent dispersing ability on the rGO (reduced graphene oxide) sheets surface (designated as rGO/Fe_3O_4/Au) to avoid adverse agglomeration between the nano particles and overlapping of the rGO sheets concurrently. The resultant bifunctional composite shows high performance in the catalytic reduction of 4-nitrophenol (4-NP) with conversion of 97% in 5 min and presents good reusability through highly efficient recovery by using external magnetic fields. In particular, there was no significant loss in catalytic activity of the reused catalysts even after being recycled for 8 cycles, displaying attractive potential applications in industrial applications where separation and recycling are imperative. The rational design provide an approach to synthesize graphene-based composite with interesting structure and multi-functional property as well.

1. Introduction

In the past decades, significant progress has been made with regard to the design, synthesis and utilization of nanostructured materials for efficient energy utilization and environment protection.[1] Among various systems, noble-metal nanostructures have received great interest due to their unique optical, catalytic and electrochemical properties which lead to a number of fascinating potential applications in electronic, chemical, biological, hydrogen storage and catalytic fields.[2] Au nanoparticles (NPs) have been proven to be highly efficient catalyst in several catalytic processes including low-temperature CO oxidation, reductive catalysis of nitrogen oxides, acetylene hydrochlorination, reduction of nitrophenol and organic synthesis. The catalyst performance of Au NPs is directly related to their size, shape and the dispersion.[3] Unfortunately, unprotected Au NPs are active and susceptible to irreversible aggregation in solution during preparation and catalytic process due to van der Waals forces and high surface energy. Certainly, irreversible aggregation of Au NPs results in substantial reduction of catalytic activity.

In order to overcome this drawback and improve the stability of Au NPs, an effective strategy to avoid the aggregation is introducing solid supports (such as silica, polymers, metal oxides, carbon materials, etc.) and then immobilizing the Au NPs on the supports to form composite catalysts.[4] Carbon materials, for example carbon nanotubes (CNTs) and graphene, have been considered as impactful support materials owing to their high surface area, excellent loading capacity, appropriate pore sizes and abundant accommodation for NPs.[5] Among them, support materials based on two dimensional (2D) reduced graphene oxide (rGO) has especially fascinated the scientific community due to their high electrical conductivity, large specific surface area, flexible structures and mechanical robustness.[6] RGO presents outstanding capability of accommodating volume changes during reaction and displays advantage in loading of the metal or metal oxides for potential applications in various fields.[7] Moreover, this metal/metal oxides loading process can not only prevent graphene sheets from restacking but also improve the catalytic performance beneficial from the strong synergistic interaction between the two components.[8] Furthermore, the strong covalent interfacing of the metal/metal oxides with graphene could also significantly reduce catalyst poisoning. Consequently, composite catalysts based on graphene loaded with metal/metal oxides exhibit high catalytic property as well as good mechanical stability. There have been many efforts toward synthesizing highly dispersed Au NPs and assembling them on graphene to form different nanostructures. For instance, Li et al. synthesized Au/graphene composite under hydrothermal conditions through the self-assembly process. Exhibited excellent catalytic performance towards the reduction of 4-NP to 4-Aminophenol (4-AP), which is ariseing from the synergistic effect of graphene with Au NPs.[9] Yao and co-workers recently developed a method to achieve self-assembly of Au NPs on graphene sheets through chemical functionalization. These graphene/Au composites display good stability against

School of Opto-electronic Information, University of Electronic Science and Technology of China, 610054 Chengdu, China
E-mail:wangyan127@uestc.edu.cn

Electronic Supplementary Information (ESI) available: [details of any supplementary information available should be included here]. See DOI: 10.1039/x0xx00000x

agglomeration and show excellent catalytic activity in reduction of 4-NP into 4-AP.[10] Moreover, graphene-based composite catalysts such as graphene/Co_3O_4, graphene/$MnCo_2O_4$ and graphene/MoS_2 have been studied as composite catalysts for environmental purification.[11] In these cases, graphene serve as support for the metal or metal oxides NPs. The graphene/NPs composites can not only alleviate the aggregation problem of the NPs and the restacking of the graphene, but also facilitate the electron transfer between the NPs and graphene during the catalytic process and improve the chemical stability as well. Although progress has been made, significant challenges remain in how graphene-based composite catalysts can be separated from the reaction solution and recycled further. Solving this problem is thus critical for their application in environmentally friendly process. Therefore, it is significant to develop well-defined nanostructure catalyst materials with high surface area and unique separable features to enable convenient recycling. In this regard, integrating magnetic particles into the graphene-based catalyst composite as a magnetically recoverable catalyst support could be a promising solution.

In this work, we report a multifunctional catalyst composite with both magnetism and catalytic activity, which is synthesized by a hydrothermal method for the first time. GO sheets were modified by silica and they acted as the support for nanoparticles. The silica-modified GO sheets promoted the dispersing of Fe_3O_4 particles on graphene sheets during the simple in situ growth hydrothermal reaction using ferric acetylacetonate ($Fe(acac)_3$) as precursor. And then the Au NPs were evenly assembled to the as-prepared rGO/Fe_3O_4 by a hydrothermal method. The resulting product is designated as rGO/Fe_3O_4/Au. The synthesis offers good controllability of the size and dispersion of Fe_3O_4 and Au NPs with high-yield. The designed composite catalyst shows excellent dual functions: one is high catalytic efficiency towards the reduction of 4-NP (with conversion of 97% in 5 min) in the presence of $NaBH_4$; another is easy recyclability by using an external magnetic field without significant decrease in the catalytic performance after 8 reuses.

2. Experimental Section

All materials including natural graphite, cetyltrimethyl ammonium bromide (CTAB), ethanol, sodium hydroxide (NaOH), tetraethoxysilane (TEOS), concentrated ammonia solution (25 wt%), $HAuCl_4$, sodium citrate, tannic acid, $NaBH_4$ and 4-NP are of analytical grade and were purchased from Sinopharm Chemical Reagent Co., Ltd. (China) and used as received without further purification.

2.1. Synthesis of the silica modified GO.

Graphite oxide (GO) was prepared from natural graphite by a modification of the Hummers method.[12] The GO solution was prepared by dispersing GO in deionized water under sonication.

In a typical procedure, the silica modified graphite oxide sheets were prepared by hydrolysis of TEOS in an alcohol medium in the presence of water and ammonia by a modification of the Stöber method. 20 mg NaOH and 0.5 g CTAB were dispersed in 20 mL GO solution (1 mg/mL) ultra-sonication for 2 h at room temperature. The mixed solution was maintained at 40°C in a water bath for 2 h and 1.2 mL TEOS was added drop-wise into the above solution with vigorous stirring. After another 12 h stirring, the precipitates (silica modified GO) were filtered and washed several times with deionized water and dried at 80°C under vacuum for 6 h.

2.2. Synthesis of the rGO/Fe_3O_4 composite.

20 ml deionized water and 0.08 g $Fe(acac)_3$ were added into the above collected silica modified GO in turn and the mixed solution was stirred for 30 min, the pH value of the mixed solution was adjusted to 11 by ammonia solution (25 %). After additional agitation for 5 min, the resultant solution was transferred into a 50 mL autoclave, sealed and heated at 220°C for 12 h, followed by washing with deionized water and drying at 60°C in air overnight. Finally the rGO/Fe_3O_4 composite was prepared.

2.3. Synthesis of rGO/Fe_3O_4/Au composite.

The Au NPs on GO surface with a diameter of about 10 nm were prepared by the citrate reduction method in the presence of tannic acid. 0.4 mL of 1 g/L $HAuCl_4$ was mixed with 30 mL deionized water containing 0.04 g sodium citrate and 0.02 g tannic acid and kept in a water bath at 60°C for 4 h. The as-prepared rGO/Fe_3O_4 composite was dispersed in the above solution and stirred for 30 min. Finally, the resulting rGO/Fe_3O_4/Au composite was separated by centrifugation, rinsed with ethanol and dried at room temperature.

The rGO/Fe_3O_4/Au composite using GO only to anchor Fe_3O_4 and Au was prepared by the similar process without the modification of silica on the GO surface.

2.4. Catalytic reaction.

The reduction of 4-NP compound by rGO/Fe_3O_4/Au composite in the presence of $NaBH_4$ was carried out to examine the catalytic activity and recyclability of the rGO/Fe_3O_4/Au composite catalyst. For comparison, the yellow aqueous 4-NP solution (0.08 M) was prepared and measured prior to monitoring the changes of absorption. A total of 50 µL 4-NP solution (5 mM) was mixed with 1.0 mL of fresh $NaBH_4$ aqueous solution (0.2 M). Subsequently, 2.0 mL ultrapure water was swiftly added to the solution and it turned from light yellow to bright yellow immediately. Then 4 mg rGO/Fe_3O_4/Au composite catalyst was added to the solution. The above solution was quickly subjected to UV-vis measurements, therefore, the obtained data can be designated as the value for reaction time t = 0. Changes in the concentration of 4-NP were monitored by UV-vis spectroscopy at room tempe rature. In fact, as the reaction proceeds, the color of the mixture gradually vanished, indicating the reduction of the 4-NP. To study the reusability of the rGO/Fe_3O_4/Au composite catalyst, the used samples were separated from the solution with a magnet after the monitoring of the whole reduction process was completed. The recycled magnetic microspheres were washed with

ethanol 6 times and with deionized water 3 times for the next cycle. Similar to the above reduction process, the obtained rGO/Fe_3O_4/Au composite was redispersed with 2.0 mL of deionized water and mixed with 0.05 mL of aqueous 4-NP solution (0.005 M) and 1.0 mL of fresh $NaBH_4$ (0.2 M) solution. With a stiff limit of 5 min kept for completion of the reaction, the solution was measured using UV-vis spectroscopy. The procedure was repeated 8 times and no significant decrease in the 4-NP conversion was detected.

2.5. Characterization.

X-ray diffraction (XRD) patterns were collected on a Rigaku D/max-TTR-III diffractometer using Cu Kα radiation (λ = 0.15405 nm). Raman spectra were measured on a Renishaw RM2000 Raman spectrometer with 457.9 nm wavelength incident laser light. The X-ray photoelectron spectra (XPS) measurements were performed by using a VG ESCALAB MK II electron energy spectrometer using Mg Ka (1253.6 eV) as the X-ray excitation source. The morphologies of the as-prepared nanocomposites were inspected on the scanning electron microscope (SEM, JSM-6480A, Japan Electronics), energy dispersive X-ray (EDX) and transmission electron microscopy (TEM). The high-resolution transmission electron microscopy (HRTEM) micrographs were acquired on a FEI Tecnai G^2 S-Twin transmission electron microscope with a field emission gun operating at 200 kV. N_2 adsorption/desorption isotherms were measured at a liquid nitrogen temperature (-196°C) using a Micromeritics ASAP 2010 instrument. The specific surface area was calculated by the Brunauer-Emmett-Teller (BET) method. FT-IR spectra were measured on a Perkin-Elmer 580BIR spectrophotometer using KBr technique. The absorbance of 4-NP was obtained on a TU-1901 UV/vis spectrophotometer. The samples were placed in a 1 cm × 1 cm × 3 cm quartz cuvette and the spectra were recorded at room temperature. Magnetization measurements were performed on a MPM5-XL-5 superconducting quantum interference device (SQUID) magnetometer at 300 K.

3. Results and discussion

3.1. Morphology, structure, phase and textural Properties.

The crystal structures of the pure GO, rGO/Fe_3O_4 and rGO/Fe_3O_4/Au composites were characterized by XRD and shown in Fig. 1. The XRD pattern of the GO consists of one major peak around 10°, which is in good agreement with the reported results and confirms that GO was successfully synthesized from graphite by the modified Hummers method.[13] Four resolved peaks at 2θ = 19.09°, 31.25°, 36.8° and 59.3° in the XRD pattern of rGO/Fe_3O_4/Au composite, can be indexed into the fcc Fe_3O_4 structure. While the peaks at 2θ = 38.4°, 44.6°, 65° and 77.3° are commonly observed inthe ace-centered cubic structured Au NPs XRD patterns. The sharp and strong peaks confirm that the Fe_3O_4 and Au are highly crystallized. The XRD pattern of the rGO/Fe_3O_4/Au composite matches well with the corresponding JCPDS standards of Fe_3O_4 and Au (JCPDS 22-1136; JCPDS 04-0784), indicating that both

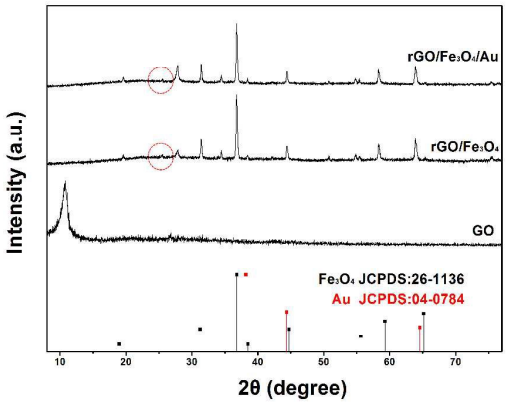

Fig. 1. XRD patterns of the pristine GO, rGO/Fe_3O_4 and the rGO/Fe_3O_4/Au composite.

the Au NPs and Fe_3O_4 were successfully located onto GO sheets. Because the diffraction peaks for Au are similar with Fe_3O_4. More evidence to prove the successful load of Au NPs were shown in the discussion in Fig. 3. For the XRD pattern of rGO/Fe_3O_4 composite, the broad XRD peak around 25° which is indicated by the red circle could be ascribed to the (002) plane of the reduced graphene. Moreover, the disappearance of the GO peak at 2θ = 9.9° confirms the reduction of GO to rGO in the composite which indicating that the GO was reduced to rGO by thermal reduction during the preparing of rGO/Fe_3O_4 composite. The typical features of graphene are also observed in the TEM images described below.

Raman spectroscopy were used to gain information on the structure of the graphene sheets in the rGO/Fe_3O_4/Au composite and the GO. In Fig. 2, two intense peaks are clearly displayed at 1350 cm^{-1} (D band) and 1590 cm^{-1} (G band) in the Raman spectrum of the rGO/Fe_3O_4/Au composite and GO.[14] It is well known that the peak intensity ratio of the D and G band (I_D/I_G) could be used to estimate the disorder degree and average size of the sp^2 domains of the graphite structure.[15] In our experiment, the I_D/I_G of rGO/Fe_3O_4/Au composite increases compared with that of GO. The increased I_D/I_G ratio (1.11 for rGO/Fe_3O_4/Au and 1.04 for GO, respectively) is likely

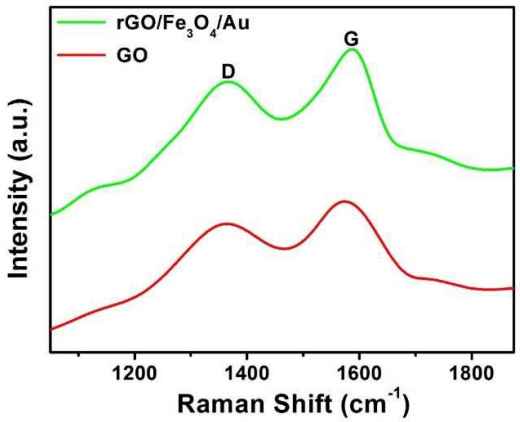

Fig. 2. Raman spectra of the pristine GO sheets and rGO/Fe_3O_4/Au composite.

due to the decrease in the size of the sp^2 graphitic domains during the preparation process and the occurrence of more defects in the graphite structure by reduction process.

X-ray photoelectron spectroscopy (XPS) was used to study the surface chemistry of the prepared reduced graphene oxide based composite. Fig. 3A shows XPS spectra of the rGO/Fe_3O_4/Au c omposite and GO. Compared with the pristine graphene sheets, the survey spectrum of the rGO/Fe_3O_4/Au prominently shows carbon, oxygen, Au and iron species. In the survey region (0−1200 eV), the peak located at 285 eV is ascribed to the characteristic peak of C 1s, which can be divided into several peaks further. As seen from Fig. 3B, deconvolution of the C 1s spectrum of rGO/Fe_3O_4/Au indicates the presence of nonoxygenated carbon at 284.8 eV, carbon in C−O (hydroxyl and epoxy groups) at 285.6 eV, C=O (carbonyl groups) at 287.1 eV and O−C=O (carboxyl groups) at 288.5 eV. XPS C 1s data for reduced graphite oxide show considerable restoration of the sp^2 hybridized carbon atoms (C–C) after reduction by citrate, demonstrating that the GO has been well deoxygenated to form graphene (Fig. S1). In addition, the presence of the ferriferrous oxidation state is confirmed from the multiplet splitting of the Fe 2p peak, as shown in Fig. 3C. Two predominant band peaks at 711.2 eV and 723.8 eV can be assigned to Fe ($2p_{3/2}$) and Fe ($2p_{1/2}$), respectively, confirming the oxidation state of Fe_3O_4 in the composite. The Au 4f peaks at the binding energies of 84.1 and 87.8 eV, as shown in Fig. 3D, are attributed to the Au $4f_{7/2}$ and Au $4f_{5/2}$, respectively. The two strong Au characteristic peaks suggest clearly the formation of the Au NPs in rGO/Fe_3O_4 with good crystallization. These results are also consistent with the XRD and Raman analysis as described above.

Fig. 4 shows the TEM images and morphology sketch of the GO modification process which plays an important role in the growth of Fe_3O_4 and deposition of Au NPs. GO nanosheets shown in Fig. 4A illustrate the success of preparing GO by

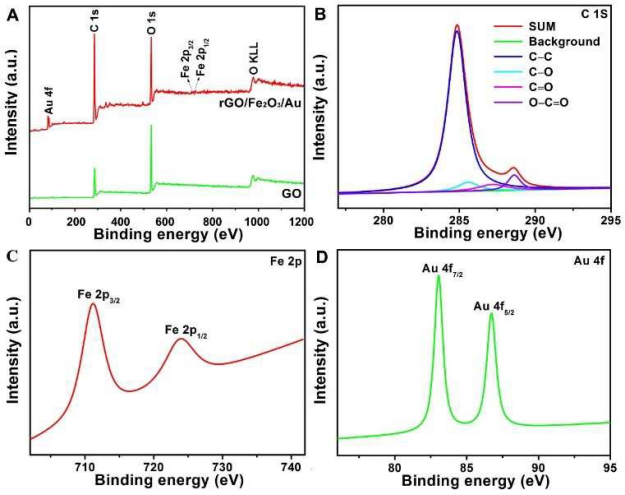

Fig. 3. XPS spectra of the pure GO sheets and as-prepared rGO/Fe_3O_4/Au composite. XPS survey spectra (A), C1s spectrum of rGO/Fe_3O_4/Au (B), Fe 2p spectrum of rGO/Fe_3O_4/Au composite (C) and Au 4f spectrum of the rGO/Fe_3O_4/Au composite (D).

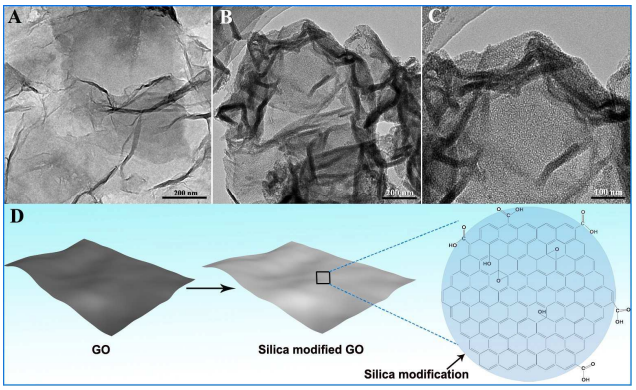

Fig 4. TEM images of GO (A), low- (B) and high-magnification (C) TEM images of silica modified GO. Schematic illustration for the silica modification process (D).

Hummers method. The GO sheets are measured to be range from approximately 1 to 4 μm in lateral dimensions. The characteristics of 2D GO with a slightly curved and crinkled texture are observed. As shown in Fig. 4B, compared with GO sheets, the 2D surface of modified GO has a relatively rough surface after the silica modification reaction. Furthermore, the magnified TEM image of silica modified GO sheets makes clearly that the GO exhibits a curly morphology with a thicker and wrinkled structure which is very likely due to the modification of silica on the surface of the GO (Fig. 4C). The modified GO sheets have more functional groups located on the GO sheets. These functional groups ensure mechanically

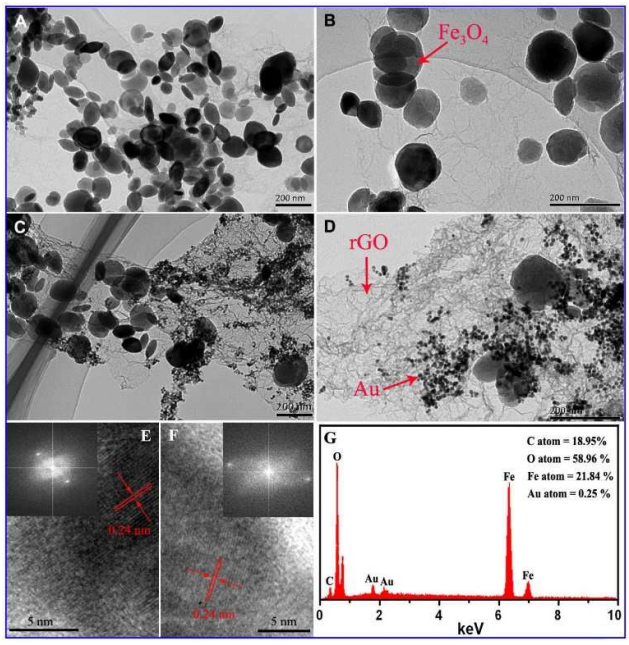

Fig. 5. Low- (A) and high-magnification (B) TEM images of rGO/Fe_3O_4 composite, low- (C) and high-magnification (D) TEM image of rGO/Fe_3O_4/Au composite, HRTEM image of rGO/Fe_3O_4/Au composite (E, F) and EDS (G). The insets in (E) and (F) are corresponding FFT patterns.

steady bonding between GO and ions or inorganic particles and certainly, acts as anchors for adsorption of $HAuCl_4$ and $Fe(acac)_3$ in this work (Fig. 4D).

The morphologies of the rGO/Fe_3O_4 composite and rGO/Fe_3O_4/Au composite were determined by SEM and TEM. Fig. 5A demonstrates obviously that Fe_3O_4 particles have been successfully located onto GO. A high magnification TEM image further reveals that the Fe_3O_4 particles are well dispersed on the GO sheets, as marked by the red arrow in the corresponding TEM image in Fig. 5B. For the rGO/Fe_3O_4 composite, GO exhibits a curly morphology with a thin, wrinkled structure. Notably, the decoration of the GO sheets by Fe_3O_4 particles increases the surface area and avoids the agglomeration of the Fe_3O_4 particles. Panels C and D in Fig. 5 show the TEM images of rGO/Fe_3O_4/Au composite, exhibiting obviously the formation of Au NPs on the surface of rGO after in situ reduction of $HAuCl_4$. The reduction process by the citrate allows the in situ growth of Au NPs on the graphene sheets and then attachment onto the graphene sheet stably. A high magnification TEM image of the rGO/Fe_3O_4/Au composite (see in Fig. 5D) further reveals that the Au NPs are spherical in shape and have diameters ranging from 6 nm to 15 nm. Interestingly, the rGO sheets keep in well spreading without agglomeration and with reasonably large surface area which provides a better access for the liquid into the entire structure. In the HRTEM images (Fig. 5E and F), the measured lattice spacings of 0.24 nm and 0.24 nm match well with the d_{311} spacing of the Fe_3O_4 phase and d_{111} spacing of Au, respectively. This is also supported by the corresponding fast Fourier transform (FFT) pattern in the inset. In addition, the corresponding elemental mapping picture displays a clear elemental distribution of C, O, Fe and Au elements (Fig. 5G).

Fig. 6 shows the N_2 adsorption–desorption isotherms and pore size distribution of rGO/Fe_3O_4/Au composite. According to the IUPAC classification, the sample exhibits typical IV type isotherms with an inconspicuous hysteresis loop observed in the range of 0.5-1.0 P/P_0, indicating a mesoporous nature. As expected for the observed porous nature, our rGO/Fe_3O_4/Au composite has a large specific surface area of 102.6 m^2/g, with a unimodal pore-size of 7 nm calculated by the Barrett–Joiner–Halenda (BJH) method.

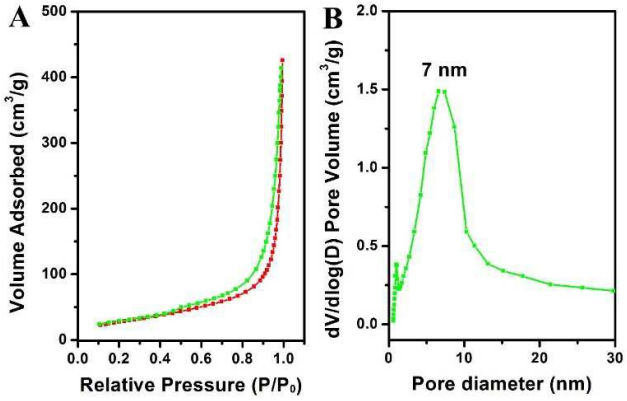

Fig. 6. N_2 adsorption/desorption isotherms (A) and particle size distribution (B) of rGO/Fe_3O_4/Au composite.

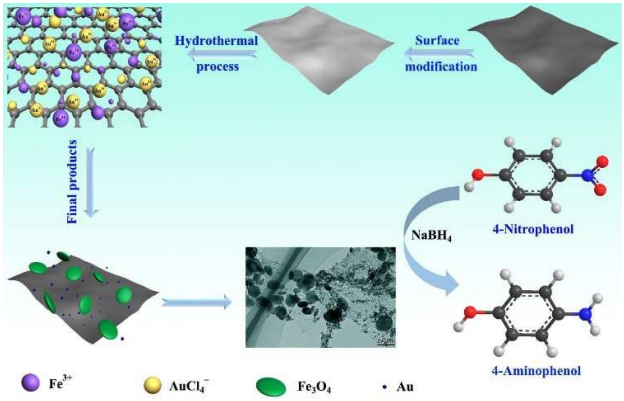

Scheme 1. Schematic illustration of the formation process of rGO/Fe_3O_4/Au composite.

The possible mechanism involved in the formation process of the rGO/Fe_3O_4/Au composite nanostructure is proposed and a representative schematic is illustrated in Scheme 1. Experimentally, construction of the composite material began with the silica modification of the GO. In GO water solution, epoxy and hydroxyl groups covered on GO surface, while carbonyl and carboxyl groups were located atthe edges. These functional groups acted as anchor sites and enabled the subsequent modification of the GO sheets. With the addition of CTAB, the GO strongly interacted with CTAB molecules and formed the capped GO sheets which can be stabilized in deionized water with excellent dispersibility. Excellent dispersibility played a key role in the following GO modified homogeneously by silica process which were accomplished by the hydrolysis of TEOS according to the Stöber method. The silica-coated GO sheets effectively avoided the aggregation of the GO sheets. Furthermore, this created negatively charged surface Si–OH groups on GO sheets. Certainly, negative charge groups could adsorb efficiently positive charge ions efficiently in the continued process. Moreover, the large surface area associated with the silica modification ensures the silica surface to immobilize a large number of ions during the following in situ growth process. After the silica modified GO and $Fe(acac)_3$ were mixed with deionized water and react under a heat treatment conditions, the Fe_3O_4 seeds were formed on the GO sheets due to the $Fe(acac)_3$ hydrolysis under alkaline condition and further in situ grown on the GO sheets to form the homogeneous rGO/Fe_3O_4 composite. Moreover, silica was removed under alkaline conditions after the reaction which is confirmed by the FT-IR spectra of GO, silica modified GO and rGO/Fe_3O_4/Au in Fig. S2. In Fig. S2, for GO, the strong band of OH (3430 cm^{-1}) and H_2O (1620 cm^{-1}) indicates that there are a large number of OH groups and H_2O present on the surface. After the silica was modified on GO sheets, several broad absorption bands assigned to OH (3430 cm^{-1}), Si-O-Si (803 cm^{-1}), Si–OH (950 cm^{-1}), and Si–O (455 cm^{-1}) groups are detected, which can be attributed to the amorphous mesoporous silica.[16] The strong absorption bands around 2920 cm^{-1} and 2850 cm^{-1} were assigned to the stretching of the C–H bonds of the CTAB

molecules residues on the silica. After the hydrothermal reaction, the silica was removed. Notably, GO was reduced to rGO by thermal reduction and most of the oxygen-containing groups on GO sheets are removed. After that, rGO/Fe_3O_4 was react with citrate-capped $AuCl_4^-$ solution for the reduction of $AuCl_4^-$ to Au NPs form the rGO/Fe_3O_4/Au composite nanostructure. The functional groups present on the surface of the GO was dispeared for the rGO/Fe_3O_4/Au sample. The process can be described as an in situ decoration of Au NPs on the surface of rGO/Fe_3O_4. The two important reactions improve greatly the electrochemical property of the rGO/Fe_3O_4/Au composite. In addition, citrate served as a reducing agent for the synthesis of Au NPs as well as a chelating ligand with strong coordinating ability to coordinate with Au and rGO/Fe_3O_4 composites to form stable complexes.

RGO/Fe_3O_4/Au composite obtained by our facile approach show many unique advantages in comparison with conventional catalysts. Firstly, this advanced in situ growth and reduction method achieved a tight decoration of Fe_3O_4 and Au NPs on rGO support; the tight decoration ensures rGO/Fe_3O_4/Au to keep quite good stability in catalytic reaction, as well as in magnetic recycling. Secondly, well-crystallized Fe_3O_4 and Au NPs are evenly prepared and specially dispersed on the rGO supports with a narrow size distribution. This novel structure can effectively prevent nano particles and nano sheets from aggregation in close proximity even at high particle densities. Thirdly, it is feasible to grow two or more kinds of nano particles on nano sheet surface simultaneously to play different roles, for example in this report, the Au NPs act as a high performance catalyst and the decorated Fe_3O_4 nano particles made the composite convenient for recycling. Consequently, inorganic nanostructured catalysts with high surface area, magnetic property, facile regeneration and catalytic performance are reserved, which is important for the super catalytic activity.

3.2. Catalytic performance of the rGO/Fe_3O_4/Au composite

The reduction of 4-NP to 4-AP by $NaBH_4$ process is monitored by tracking the changes in the absorbance peak on the UV/vis spectra at different times. The addition of sodium borohydride in 4-NP resulted in a yellow aqueous solution and an absorption maximum located at 400 nm (Fig. 7A-C) due to the formation of 4-nitrophenolate ion. Fig. 7A illustrates a blank test conducted with a mixture of 4-NP and $NaBH_4$, without rGO/Fe_3O_4/Au composite. No change in the color of the reaction mixture or the absorption peak intensity was observed even after standing for 12 h, which states clearly that the reduction of 4-NP did not occur without the introduction of the catalyst. After addition of a small amount (4.0 mg) of the rGO/Fe_3O_4/Au composite, the reduction commenced and absorption peak at 400 nm significantly decreased as the reaction proceeds. Meanwhile, a new peak appears at 295 nm, which is corresponding to 4-AP increases, reveals surely the reduction of 4-NP to form 4-AP (Fig. 7B). After an 5 min reduction reaction, the pristine bright yellow solution faded to completely colorless and no characteristic absorption of nitro compound could be detected at 400 nm, which proved that

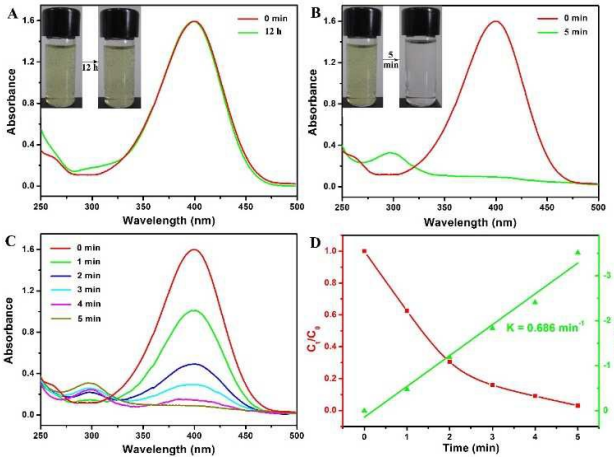

Fig. 7. UV-vis spectra of the catalytic reduction of 4-NP to 4-AP developed at different reaction times when no catalyst was added (A), UV-vis spectra of the catalytic reduction of 4-NP to 4-AP developed at different reaction times using 4 mg rGO/Fe_3O_4/Au composite (B); UV-vis spectra of the catalytic reduction of 4-NP to 4-AP developed at different reaction times (C); C_t/C_0 and $\ln(C_t/C_0)$ versus time for the reduction of 4-NP over 4 mg rGO/Fe_3O_4/Au catalyst, The ratio of 4-NP concentration (C_t at time t) to its initial value C_0 is directly represented by the relative intensity of the respective absorption peak at 400 nm.

the catalytic reduction of 4-NP had proceeded successfully (Fig. 7C). The mechanism of catalytic reduction of 4-NP to 4-AP is explained in details in Fig. 8. The catalytic reduction of 4-NP to 4-AP occurred via relaying of electrons from the BH^{4-} donor to the acceptor 4-NP. When the rGO/Fe_3O_4/Au catalyst composite was added into the reaction mixture, the BH^{4-} ions as well as the 4-NP were adsorbed on the surface of catalyst and transfer a surface-hydrogen species to the surface of the Au NPs, leading to the rapid occurrence and completion of the reduction reactions. The rate of reduction reaction catalyzed

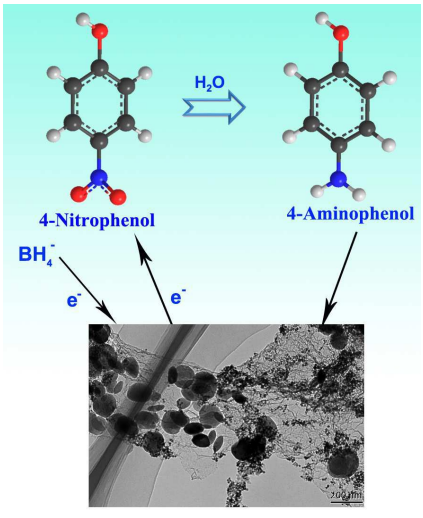

Fig. 8. Mechanism of catalytic reduction of 4-NP.

by rGO/Fe_3O_4/Au composite was assumed to be independent of the concentration of $NaBH_4$ because the initial concentration of the $NaBH_4$ solution is excessed compared to 4-NP. Therefore, a pseudo first-order kinetic equation can be applied to evaluate the catalytic rate, denoted as

$$-dC/dt = dA/dt = kC_t = kA_t \quad (1)$$

$$\ln(C_t/C_0) = \ln(A_t/A_0) = -kt \quad (2)$$

where C_t is the concentration of 4-NP at time t and k is the apparent rate constant. The ratio of C_t to C_0 is measured from the relative intensity of absorbance (A_t/A_0) at 400 nm. Fig. 7D shows the relation of $\ln(C_t/C_0)$ versus time t. The clearly linear relationship between $\ln(C_t/C_0)$ and t indicates that the reduction of 4-NP by rGO/Fe_3O_4/Au composite matches well with the pseudo-first-order and the rate constant k is calculated to be 0.686 min^{-1}, and the turnover frequency (TOF) of the rGO/Fe_3O_4/Au composite for the catalytic reaction of 4-NP was calculated to be 716 h^{-1}.

To investigate the reusability, the rGO/Fe_3O_4/Au composite was separated using a magnet from the catalytic reaction solution and the cyclic stability was recorded. Fig. 9A shows the magnetization curve of rGO/Fe_3O_4/Au at room temperature. The saturation magnetization value is 8.0 emu/g. The inset photographs in Fig. 9A demonstrates the easy separation of rGO/Fe_3O_4/Au by an external magnetic field in 30 s and states clearly the reusability of rGO/Fe_3O_4/Au catalyst. The reusability test result of rGO/Fe_3O_4/Au composite, as shown in Fig. 9B, further confirms that the catalyst exhibits similar catalytic performance without visible reduction (decreased less than 10%) even after running for 8 cycles, which suggested an excellent stability and long life of as-prepared rGO/Fe_3O_4/Au catalyst.

The good catalytic activity of rGO/Fe_3O_4/Au composite could be explained from three aspects. First, highly dispersed Au NPs were decorated on the surface of rGO sheets to make sure Au NPs in high catalytic activities. In addition, each nanoparticle isolated on rGO sheets has a relatively homogeneous environment around the particle surface thus leading to a high rate of reduction. Second, the good mechanical stability, excellent conductivity property and large surface area derived from rGO, as well as its porous characteristic are expected to have favorable functions for the excellent catalytic properties of the rGO/Fe_3O_4/Au composite.

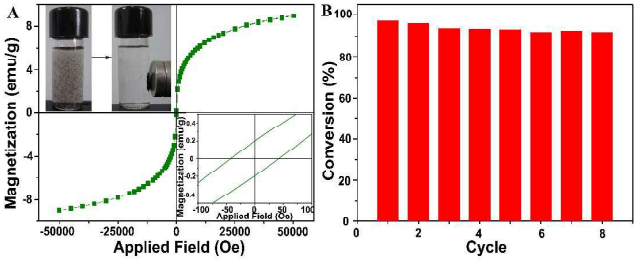

Fig. 9. Magnetization curve of rGO/Fe_3O_4/Au at room temperature (A), The inset shows the photographs of the magnetic separation. The reusability of rGO/Fe_3O_4/Au catalyst (B).

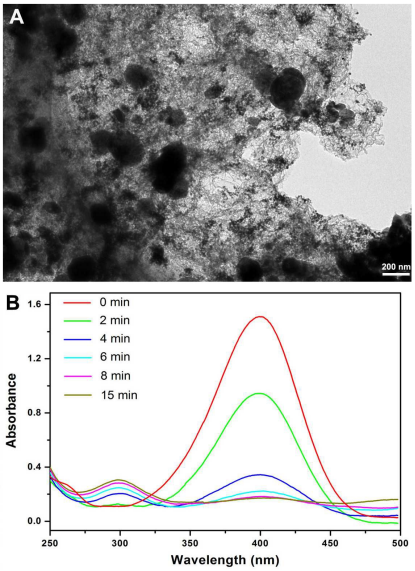

Fig. 10. TEM image of rGO/Fe_3O_4/Au composite using GO only to anchor Fe_3O_4 and Au (A). UV-vis spectra of the catalytic reduction of 4-NP to 4-AP developed at different reaction times for the sample (B).

Third, the interaction between Au NPs and rGO supports is more effective than that of the bulk forms, which facilitate the electron transfer between the Au NPs, thus the rGO sheets can provide more active sites to adsorb and reduce 4-NP. Apparently, the synergetic effects between Au NPs and rGO improve catalytic property of rGO/Fe_3O_4/Au composite greatly. Importantly, the good dispersion of Fe_3O_4 and Au particles is ascribed to the silica-coated GO sheets which can effectively avoided the aggregation of the GO sheets. The abundant surface groups on silica modified GO ensures the surface to immobilize a large number of ions during the particles decorating process. In order to clarify the crucial role the silica modified graphene surface played in the particles decorating process, the rGO/Fe_3O_4/Au composite using GO only to anchor Fe_3O_4 and Au was prepared by the similar process without the modification of silica on the GO surface. And, the catalytic property of the composite is demonstrated in Fig. 10 which shows a low performance in the catalytic reduction of 4-NP with conversion of 88 % in 15 min. The relatively low catalytic performance of the composite which using GO only to anchor Fe_3O_4 and Au may ascribed to the morphology property of the composite. As shown in Fig. 10, in contrast to the good dispersion and high loading amount of the Fe_3O_4 and Au particles in the rGO/Fe_3O_4/Au composite which using silica modified GO to anchor particles, agglomeration property of the graphene and low loading of particles are observed for the composite using GO only to anchor Fe_3O_4 and Au, which may result in the inferior catalytic characteristics.

Conclusions

In summary, rGO/Fe_3O_4/Au composite with highly dispersed Au NPs and Fe_3O_4 particles have been synthesized with high yield by a facile hydrothermal method firstly. The as-prepared rGO/Fe_3O_4/Au composite possesses high surface area, good dispersity of Au NPs and active interaction between Au NPs and rGO supports, thus exhibiting high catalytic performance demonstrated strongly by the reduction of 4-NP to 4-AP by $NaBH_4$. In addition, the rGO/Fe_3O_4/Au composite can be conveniently separated from reaction solution using external magnetic fields and the recovered composite presents excellent reusability. Finally, we believe that the promising synthetic strategy can be extended to develop other graphene based different metal or metallic compounds decorated composites for various applications in fields of catalysis, optical devices, sensors and alkaline secondary batteries.

Acknowledgements

Financial support from the National Natural Science Foundation of China (NSFC 61071027) and the Fundamental Research Funds for the Central Universities of China (ZYGX2015KYQD014) is greatly acknowledged.

References

1 (a) C. J. Liu, U. Burghaus, F. Besenbacher and Z. L. Wang, ACS Nano, Preparation and characterization of nanomaterials for sustainable energy production, 2010, 4, 5517-5526; (b) L. Jia, Y. L. Zhao and X. J. Liang, Nano Today, Fast evolving nanotechnology and relevant programs and entities in China, 2011, 6, 6-11; (c) H. L. Wang and H. J. Dai, Chem. Soc. Rev., Strongly coupled inorganic-nano-carbon hybrid materials for energy storage, 2013, 42, 3088-3113; (d) A. S. Arico, P. Bruce, B. Scrosati, J. M. Tarascon and W. Van Schalkwijk, Nat. Mater., Nanostructured materials for advanced energy conversion and storage devices, 2005, 4, 366-377; (e) V. Biju, Chem. Soc. Rev., Chemical modifications and bioconjugate reactions of nanomaterials for sensing, imaging, drug delivery and therapy, 2014, 43, 744-764; (f) X. J. Zhou, J. L. Qiao, L. Yang and J. J. Zhang, Adv. Energy Mater., A review of graphene-based nanostructural materials for both catalyst supports and metal-free catalysts in PEM fuel cell oxygen reduction reactions, 2014, 4, 1301523-1301548.

2 (a) S. J. Guo and E. K. Wang, Nano Today, Noble metal nanomaterials: controllable synthesis and application in fuel cells and analytical sensors, 2011, 6, 240-264; (b) P. K. Jain, X. H. Huang, I. H. El-Sayed and M. A. El-Sayed, Acc. Chem. Res., Noble Metals on the Nanoscale: Optical and photothermal properties and some applications in imaging, sensing, biology, and medicine, 2008, 41, 1578-1586; (c) X. Zhang, X. J. Zan and Z. H. Su, J. Mater. Chem., Polyelectrolyte multilayer supported Pt nanoparticles as catalysts for methanol oxidation, 2011, 21, 17783-17789; (d) M. Schrinner, M. Ballauff, Y. Talmon, Y. Kauffmann, J. Thun, M. Moller and J. Breu, Science, Single nanocrystals of platinum prepared by partial dissolution of Au-Pt nanoalloys, 2009, 323, 617-620; (e) L. Kuai, B. Y. Geng, X. T. Chen, Y. Y. Zhao and Y. C. Luo, Langmuir, Facile subsequently light-induced route to highly efficient and stable sunlight-driven Ag-AgBr plasmonic photocatalyst, 2010, 26, 18723-18727.

3 (a) R. R. Si, J. F. Liu, K. Yang, X. Chen, W. X. Dai and X. Z. Fu, J. Catal., Temperature-programed surface reaction study of CO oxidation over Au/TiO_2 at low temperature: An insight into nature of the reaction process, 2014, 311, 71-79; (b) L. Q. Nguyen, C. Salim and H. Hinode, Appl. Catal. A, Performance of nano-sized Au/TiO_2 for selective catalytic reduction of NOx by propene, 2008, 347, 94-99; (c) M. Conte, C. J. Davies, D. J. Morgan, T. E. Davies, D. J. Elias, A. F. Carley, P. Johnston and G. J. Hutchings, J. Catal., Aqua regia activated Au/C catalysts for the hydrochlorination of acetylene, 2013, 297, 128-136; (d) A. Corma and H. Garcia, Chem. Soc. Rev., Supported gold nanoparticles as catalysts for organic reactions, 2008, 37, 2096-2126; (e) P. X. Zhao, X. W. Feng, D. S. Huang, G. Y. Yang and D. Astruc, Coord. Chem. Rev., Basic concepts and recent advances in nitrophenol reduction by gold- and other transition metal nanoparticles, 2015, 287, 114-136; (f) M. D. Hughes, Y. J. Xu, P. Jenkins, P. McMorn, P. Landon, D. I. Enache, A. F. Carley, G. A. Attard, G. J. Hutchings, F. King, E. H. Stitt, P. Johnston, K. Griffin and C. J. Kiely, Nature, Tunable gold catalysts for selective hydrocarbon oxidation under mild conditions, 2005, 437, 1132-1135; (g) A. S. K. Hashmi and G. J. Hutchings, Angew. Chem. Int. Ed., Gold catalysis, 2006, 45, 7896-7936; (h) L. Kuai, S. Z. Wang and B. Y. Geng, Chem. Commun., Gold-platinum yolk-shell structure: a facile galvanic displacement synthesis and highly active electrocatalytic properties for methanol oxidation with super CO-tolerance, 2011, 47, 6093-6095.

4 (a) P. Xiao, Y. X. Zhao, T. Wang, Y. Y. Zhan, H. H. Wang, J. L. Li, A. Thomas and J. J. Zhu, Chem. Eur. J., Polymeric carbon nitride/mesoporous silica composites as catalyst support for Au and Pt nanoparticles, 2014, 20, 2872-2878; (b) A. Buonerba, A. Noschese and A. Grassi, Chem. Eur. J., Highly efficient direct aerobic oxidative esterification of cinnamyl alcohol with alkyl alcohols catalysed by gold nanoparticles incarcerated in a nanoporous polymer matrix: a tool for investigating the role of the polymer host, 2014, 20, 5478-5486; (c) M. J. Li, Z. L. Wu and S. H. Overbury, J. Catal., CO oxidation on phosphate-supported Au catalysts: Effect of support reducibility on surface reactions, 2011, 278, 133-142; (d) Y. Mei, Y. Lu, F. Polzer, M. Ballauff and M. Drechsler, Chem. Mater., Catalytic activity of palladium nanoparticles encapsulated in spherical polyelectrolyte brushes and core-shell microgels, 2007, 19, 1062-1069; (e) Y. Lu, Y. Mei, M. Drechsler and M. Ballauff, Angew. Chem. Int. Ed., Thermosensitive core-shell particles as carriers for Ag nanoparticles: modulating the catalytic activity by a phase transition in networks, 2006, 45, 813-816; (f) M. S. Chen and D. W. Goodman, Science, The structure of catalytically active gold on titania, 2004, 306, 252-255; (g) E. Lam and J. H. T. Luong, ACS Catal., Carbon materials as catalyst supports and catalysts in the transformation of biomass to fuels and chemicals, 2014, 4, 3393-3410.

5 (a) S. Nardecchia, D. Carriazo, M. L. Ferrer, M. C. Gutierrez and F. del Monte, Chem. Soc. Rev., Three dimensional macroporous architectures and aerogels built of carbon nanotubes and/or graphene: synthesis and applications, 2013, 42, 794-830; (b) D. M. Sun, C. Liu, W. C. Ren and H. M. Cheng, Small, A review of carbon nanotube- and graphene-based flexible thin-film transistors, 2013, 9, 1188-1205.

6 (a) C. C. Huang, C. Li and G. Q. Shi, Energy Environ. Sci., Graphene based catalysts, 2012, 5, 8848-8868; (b) S. Stankovich, D. A. Dikin, G. H. B. Dommett, K. M. Kohlhaas, E. J. Zimney, E. A. Stach, R. D. Piner, S. T. Nguyen and R. S. Ruoff, Nature, Graphene-based composite materials, 2006, 442, 282-286; (c) X. Z. Zhou, X. Huang, X. Y. Qi, S. X. Wu, C. Xue, F. Y. C. Boey, Q. Y. Yan, P. Chen and H. Zhang, J. Phys. Chem. C, In situ synthesis of metal nanoparticles on single-layer graphene oxide and reduced graphene oxide surfaces, 2009, 113, 10842-10846; (d) Z. Hu, Y. D. Huang, S. F. Sun, W. C. Guan, Y. H. Yao, P. Y. Tang and C. Y. Li, Carbon, Visible light driven photodynamic anticancer activity of graphene

oxide/TiO_2 hybrid, 2012, 50, 994-1004; (e) Z. Hu, J. Li, C. Y. Li, S. J. Zhao, N. Li, Y. F. Wang, F. Wei, L. Chen and Y. D. Huang, J. Mater. Chem. B, Folic acid-conjugated graphene-ZnO nanohybrid for targeting photodynamic therapy under visible light irradiation, 2013, 1, 5003-5013.

7 (a) H. P. Cong, J. F. Chen and S. H. Yu, Chem. Soc. Rev., Graphene-based macroscopic assemblies and architectures: an emerging material system, 2014, 43, 7295-7325; (b) Q. J. Xiang, J. G. Yu and M. Jaroniec, Nanoscale, Enhanced photocatalytic H-2-production activity of graphene-modified titania nanosheets, 2011, 3, 3670-3678; (c) Y. J. Hu, J. A. Jin, P. Wu, H. Zhang and C. X. Cai, Electrochim. Acta, Graphene-gold nanostructure composites fabricated by electrodeposition and their electrocatalytic activity toward the oxygen reduction and glucose oxidation, 2010, 56, 491-500; (d) C. Nethravathi, M. Rajamathi, N. Ravishankar, L. Basit and C. Felser, Carbon, Synthesis of graphene oxide-intercalated alpha-hydroxides by metathesis and their decomposition to graphene/metal oxide composites, 2010, 48, 4343-4350; (e) X. Huang, X. Y. Qi, F. Boey and H. Zhang, Chem. Soc. Rev., Graphene-based composites, 2012, 41, 666-686; (f) X. Huang, Z. Y. Yin, S. X. Wu, X. Y. Qi, Q. Y. He, Q. C. Zhang, Q. Y. Yan, F. Boey and H. Zhang, Small, Graphene-based materials: synthesis, characterization, properties, and applications, 2011, 7, 1876-1902; (g) Y. J. Hu, H. Zhang, P. Wu, H. Zhang, B. Zhou and C. X. Cai, Phys. Chem. Chem. Phys., Bimetallic Pt-Au nanocatalysts electrochemically deposited on graphene and their electrocatalytic characteristics towards oxygen reduction and methanol oxidation, 2011, 13, 4083-4094; (h) H. B. Wang, T. Maiyalagan and X. Wang, ACS Catal., Review on recent progress in nitrogen-doped graphene: synthesis, characterization, and its potential applications, 2012, 2, 781-794.

8 (a) C. Z. Zhu and S. J. Dong, Nanoscale, Recent progress in graphene-based nanomaterials as advanced electrocatalysts towards oxygen reduction reaction, 2013, 5, 1753-1767; (b) G. P. Singh, K. M. Shrestha, A. Nepal, K. J. Klabunde and C. M. Sorensen, Nanotechnology, Graphene supported plasmonic photocatalyst for hydrogen evolution in photocatalytic water splitting, 2014, 25, 11; (c) H. Zhang, S. Chen, X. Quan, H. T. Yu and H. M. Zhao, J. Mater. Chem., In situ controllable growth of noble metal nanodot on graphene sheet, 2011, 21, 12986-12990; (d) E. O. Pentsak, E. G. Gordeev and V. P. Ananikov, ACS Catal., Noninnocent nature of carbon support in metal/carbon catalysts: etching/pitting vs nanotube growth under microwave irradiation, 2014, 4, 3806-3814.

9 J. Li, C. Y. Liu and Y. Liu, J. Mater. Chem., Au/graphene hydrogel: synthesis, characterization and its use for catalytic reduction of 4-nitrophenol, 2012, 22, 8426-8430.

10 H. Q. Yao, T. C. Huang and H. J. Sue, RSC Adv., Self-assembly of Au nanoparticles on graphene, 2014, 4, 61823-61830.

11 (a) Y. Y. Liang, H. L. Wang, J. G. Zhou, Y. G. Li, J. Wang, T. Regier and H. J. Dai, J. Am. Chem. Soc., Covalent hybrid of spinel manganese-cobalt oxide and graphene as advanced oxygen reduction electrocatalysts, 2012, 134, 3517-3523; (b) Y. G. Li, H. L. Wang, L. M. Xie, Y. Y. Liang, G. S. Hong and H. J. Dai, J. Am. Chem. Soc., MoS_2 Nanoparticles grown on graphene: an advanced catalyst for the hydrogen evolution reaction, 2011, 133, 7296-7299; (c) Y. Y. Liang, Y. G. Li, H. L. Wang, J. G. Zhou, J. Wang, T. Regier and H. J. Dai, Nat. Mater., Co_3O_4 nanocrystals on graphene as a synergistic catalyst for oxygen reduction reaction, 2011, 10, 780-786.

12 H. L. Poh, F. Sanek, A. Ambrosi, G. J. Zhao, Z. Sofer and M. Pumera, Nanoscale, Graphenes prepared by staudenmaier, hofmann and hummers methods with consequent thermal exfoliation exhibit very different electrochemical properties, 2012, 4, 3515-3522.

13 D. C. Marcano, D. V. Kosynkin, J. M. Berlin, A. Sinitskii, Z. Z. Sun, A. Slesarev, L. B. Alemany, W. Lu and J. M. Tour, ACS Nano, Improved synthesis of graphene oxide, 2010, 4, 4806-4814.

14 J. W. Lee, A. S. Hall, J. D. Kim and T. E. Mallouk, Chem. Mater., A facile and template-free hydrothermal synthesis of Mn_3O_4 nanorods on graphene sheets for supercapacitor electrodes with long cycle stability, 2012, 24, 1158–1164.

15 M. Razaul. Karim, H. Shinoda, M. Nakai, K. Hatakeyama, H. Kamihata, T. Matsui, T. Taniguchi, M. Koinuma, K. Kuroiwa, M. Kurmoo, Y. Matsumoto and S. Hayami, Adv. Funct. Mater., Electrical conductivity and ferromagnetism in a reduced graphene–metal oxide hybrid, 2012, 23, 323–332.

16 X.J. Kang , Z. Y. Cheng, D. M. Yang , P. A. Ma , M. M. Shang, C. Peng , Y. L. Dai , and J. Lin, Adv. Funct. Mater., Design and synthesis of multifunctional drug carriers based on luminescent rattle-type mesoporous silica microspheres with a thermosensitive hydrogel as a controlled switch, 2012, 22, 1470–1481.